Shell-model effective interactions calculated with chiral two- and three-nucleon forces and the Okamoto-Suzuki and Krenciglowa-Kuo iteration methods

Huan Dong[1], T. T. S. Kuo[1] and J. W. Holt[2]
[1]*Department of Physics, State University New York at Stony Brook Stony Brook, New York 11794 and*
[2]*Physik Department, Technische Universität München, D-85747 Garching, Germany*
(Dated: November 17, 2010)

We present calculations of the *sd* and *sdpf* shell-model effective interactions using the Krenciglowa-Kuo (KK) and the recently developed extended Krenciglowa-Kuo iteration method of Okamoto *et al.* (EKKO). The starting point is the low-momentum nucleon-nucleon interaction V_{low-k} obtained from the N^{3}LO chiral two-nucleon interaction. In addition we study the effects of three-nucleon forces V_{3N} on the effective interactions by including the density-dependent two-nucleon interaction derived from the leading-order chiral V_{3N} by Holt, Kaiser, and Weise. The low-energy constants c_D and c_E of V_{3N} are determined by requiring them to give satisfactory nuclear matter saturation properties. With a simple solvable model, we show that both the KK and EKKO methods are convenient for deriving the effective interactions for non-degenerate model spaces. The EKKO method is especially desirable in this situation since the vertex function $\hat{Z}$-box employed therein is well behaved while the corresponding vertex function $\hat{Q}$-box employed in the Lee-Suzuki(LS) and KK methods may have singularities. The shell-model effective interactions given by the KK and EKKO methods are equivalent to each other for both the degenerate *sd* and non-degenerate *sdpf* cases, and for the degenerate *sd* case they are both close to those given by the commonly used LS method. We suggest that the KK and EKKO methods may provide a suitable framework for deriving large-space shell-model effective interactions.

PACS numbers: 21.60.Cs, 21.30.-x,21.10.-k

I. INTRODUCTION

The nuclear shell model has provided a very successful framework for describing the properties of a wide range of nuclei. This framework is basically an effective theory [1–3], corresponding to reducing the full-space nuclear many-body problem to a model-space one with effective Hamiltonian $PH_{eff}P{=}PH_0P{+}PV_{eff}P$ where H_0 is the single-particle (s.p.) Hamiltonian and P represents the projection operator for the model space which is usually chosen to be a small shell-model space such as the *sd* shell outside an ^{16}O closed core. The effective interaction V_{eff} plays a central role in this nuclear shell model approach, and its choice and/or determination have been extensively studied, see e.g. [2–5]. As discussed in these references, V_{eff} may be determined using either an empirical approach where it is required to reproduce selected experimantal data or a microscopic one where V_{eff} is derived from realistic nucleon-nucleon (NN) interactions using many-body methods. The folded-diagram theory [1–3] is a commonly used such method for the latter. Briefly speaking, in this theory V_{eff} is given as a folded-diagram series [1–3, 6]

$$V_{eff} = \hat{Q}{-}\hat{Q}' \int \hat{Q}{+}\hat{Q}' \int \hat{Q} \int \hat{Q}{-}\hat{Q}' \int \hat{Q} \int \hat{Q} \int \hat{Q} \cdots, \tag{1}$$

where $\hat{Q}$ represents a so-called $\hat{Q}$-box, which may be written as

$$\hat{Q}(\omega) = [PVP + PVQ\frac{1}{\omega - QHQ}QVP]_L. \tag{2}$$

Here V represents the NN interaction and ω is the so-called starting energy which will be explained later (section II). Thus from the NN interaction V we can in principle calculate the $\hat{Q}$-box and thereby the effective interaction V_{eff}. Note that we use Q, without hat, to denote the Q-space projection operator. (P+Q=1.) Note also that the $\hat{Q}$-box is an irreducible vertex function where the intermediate states between any two vertices must belong to the Q space. As indicated by the subscript L in Eq.(2), $\hat{Q}$-box contains valence linked diagrams only, such as the 1st- and 2nd-order $\hat{Q}$-box diagrams for ^{18}O and ^{18}F shown in Fig.1. The $\hat{Q}'$-box of Eq.(1) is defined as ($\hat{Q}$ -PVP), namely $\hat{Q}'$ begins with diagrams 2nd-order in V. The above folded-diagram formalism has been employed in microscopic derivations of shell model effective interactions for a wide range of nuclei [2, 3].

In the present work we would like to consider two extensions for the above formalism and carry out calculations to study the effects of them. Our first extension concerns the methods employed for the calculation of the folded-diagram series as indicated by Eq.(1). The well-known Lee-Suzuki (LS) [7–9] iteration method has been commonly used in previous microscopic calculations of shell model effective interactions [2, 3]. Here we would like to employ two different methods, the Krenciglowa-Kuo (KK) iteration method [10, 11] and the newly developed extended Krenciglowa-Kuo iteration method of Okamoto, Suzuki, Kumagai and Fujii (EKKO)[12], for this calculation. As we shall discuss later, it is not convenient to use the LS method for calculating the effective

interactions for non-degenerate large model spaces such as the *sdpf* two-shell one, while both the EKKO and the KK methods can be conveniently applied in this situation. The EKKO method has an additional advantage. When the P- and Q-space are not adequately separated from each other, the $\hat{Q}$-box employed in the KK method may have singularities, causing difficulty for its iterative solution. An essential and interesting difference between the EKKO and KK methods is that the EKKO method employs the vertex function $\hat{Z}$-box while in the latter the vertex function $\hat{Q}$-box is used. This simple replacement (of $\hat{Q}$ by $\hat{Z}$) has an important advantage in circumventing the singularities mentioned above. We believe that both the EKKO and KK methods may provide a promising framework for calculating shell-model effective interactions for large model spaces (such as *sdpf* one) which may be needed for describing exotic nuclei with large neutron excess.

Another extension considered in our present work is about the inclusion of the three-nucleon force (3NF) V_{3N} in microscopic calculations of the shell-model effective interactions. Up to now most microscopic effective interaction calculations have been based on the two-nucleon interaction V_{2N} alone [2, 3]. The need of V_{3N} in nuclear many-body problems has long been recognized. The use of V_{2N} alone has been inadequate in reproducing the empirical nuclear matter saturation properties (see e.g. [13, 14] and references quoted therein). The inclusion of V_{3N} has been of essential importance in describing the binding energies and low-lying spectra of light nuclie [16–18] and in explaining the long half-life of the $^{14}C \rightarrow ^{14} N$ β-decay [19]. Otsuka et al. [21] have shown that the inclusion of V_{3N} plays a crucial role in describing the oxygen isotopes near the drip line. In the present work we shall calculate both the degenerate *sd* and the non-degenerate *sdpf* shell-model V_{eff} using the chiral N^{3}LO two-nucleon interaction [24] together with the lowest-order density dependent chiral three-nucleon force of Holt, Kaiser and Weise [19, 20]. The LS, KK and EKKO iteration methods will all be employed for the degenerate case, while using only the latter two for the non-degenedrate situation.

The organization of the present paper is as follows. In section II we shall describe a non-degenerate version of the EKKO method [12] and how we apply it and the KK method [10, 11] to shell-model effective interactions. A comparison of these two methods with the LS one [7, 8] will be made. In addition to the two-nucleon force V_{2N}, we shall include also in our calculations an effective density dependent force which is extracted from the lowest-order chiral three-nucleon force [19, 20, 23], and this inclusion will also be briefly described there. Our results will be presented and discussed in section III. We shall first perform a sequence of model calculations comparing the EKKO, KK and LS iteration methods for both degenerate and non-degenerate model spaces. Before presenting our results of shell model calculations, we shall first carry out ring-diagram calculations for symmetric nuclear matter including both V_{2N} and V_{3N}, with the parameters c_D and c_E of the three-nucleon force V_{3N} [19, 20] determined by requiring that such nuclear matter calculations reproduce satisfactorily empirical nuclear matter saturation properties. Using the V_{3N} so determined, we shall then calculate shell-model effective interactions with the nucleon-nucleon interaction given by (V_{2N}+V_{3N}) and study the effects of V_{3N}. The LS, KK and EKKO methods will all be used to calculate the degenerate *sd* effective interactions, to check if the results given by the commonly used LS method agree with the KK and EKKO ones. The KK and EKKO methods will be employed to calcualte the non-degenerate *sdpf* effecteive interactions. The influence of V_{3N} on the low-lying states of ^{18}O and ^{18}F will be discussed. A summary and conclusion will be presented in section IV.

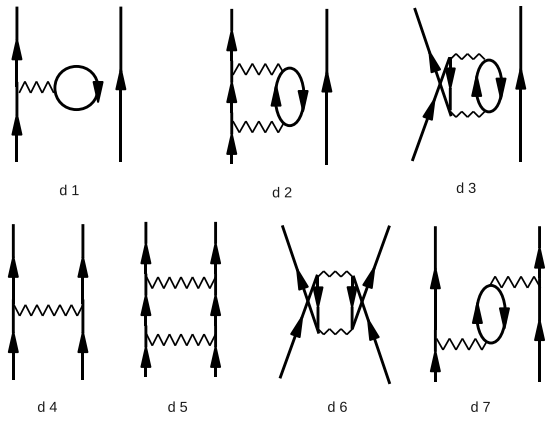

FIG. 1: Low-order diagrams constituting the $\hat{Q}$-box.

II. FORMALISM

In this section, we shall describe and discuss the KK [10, 11] and the EKKO [12] iteration methods and their application to microscopic calculations of shell-model effective interactions. These methods, to our knowledge, have not yet been employed in such calculations. Let us begin with a brief review of the LS [7, 8] and KK iteration methods. Consider first the degenerate LS method where the model space is degenerate, namely $PH_0P = W_0$, W_0 being a constant. In terms of the $\hat{Q}$-box of Eq.(2), the effective interactions R_n are calculated iteratively by [7, 8]

$$R_1 = \hat{Q}(W_0), \tag{3}$$

$$R_2 = \frac{1}{1 - \frac{d\hat{Q}}{d\omega}\mid_{\omega=W_0}} \hat{Q}(W_0), \tag{4}$$

and

$$R_n = \frac{1}{1 - \hat{Q}_1 - \sum_{m=2}^{n-1} \hat{Q}_m \prod_{k=n-m+1}^{n-1} R_k} \hat{Q}(W_0) \tag{5}$$

where the derivatives are

$$\hat{Q}_m = \frac{1}{m!}\frac{d^m\hat{Q}}{d\omega^m}\mid_{\omega=W_0}. \quad (6)$$

The effective interaction is given by the converged R_n, namely

$$V_{eff} = R_{n+1} = R_n. \quad (7)$$

There is a practical difficulty for the above iteration method. In actual shell-model calculations, it is usually not possible to calculate the vertex function $\hat{Q}$-box exactly; thus it is a common practice to evaluate it with some low-order approximations and calculate the derivatives $\hat{Q}_m$ by numerical differentiation, which is often a delicate undertaking and not accurate when m is large, say $m > 5$. As a result, the above iteration is in practice limited to low orders where numerical differentiations are reliable. (As we shall demonstrate in section IIIa, low-order LS iterations are often not accurate when P- and Q-space are strongly coupled.)

The above degenerate LS iteration method can be generalized to a non-degenrate one [9], namely PH_0P being non-degenerate. In this situation, in addition to the $\hat{Q}$-box of Eq.(2), we now also need the generalized $\hat{Q}$-box defined as

$$\hat{Q}_n(12\cdots(n+1)) = (-1)^n[PVQg_1^Qg_2^Q\cdots g_{n+1}^QQVP]_L. \quad (8)$$

with

$$g_\alpha^Q \equiv \frac{1}{\epsilon_\alpha - QHQ}. \quad (9)$$

In the above $\hat{Q}_n(1,2,\cdots,(n+1))$ is for $n \geq 1$, ϵ_α is defined by $PH_0P\phi_\alpha = \epsilon_\alpha\phi_\alpha$, and $P = \Sigma_{m\leq d}P_m$ and $P_m = |\phi_m\rangle\langle\phi_m|$. The dimension of the P-space is labelled d. Note that only valence-linked diagrams are retained in $\hat{Q}_n(\epsilon_1,\cdots,\epsilon_{n+1})$, as indicated by the subscript L.

With the above definitions, the effective interaction given by the degenerate LS iteration method is given as [9]

$$\begin{aligned}
R_1 &= \sum_\alpha \hat{Q}(\epsilon_\alpha)P_\alpha,\\
R_2 &= \sum_\alpha\left[1-\sum_\beta \hat{Q}_1(\alpha\beta)P_\beta\right]^{-1}\hat{Q}(\epsilon_\alpha)P_\alpha,\\
R_3 &= \sum_\alpha\left[1-\sum_\beta \hat{Q}_1(\alpha\beta)P_\beta - \sum_{\beta\gamma}\hat{Q}_2(\alpha\beta\gamma)P_\beta R_2 P_\gamma\right]^{-1}\\
&\quad\times\hat{Q}(\epsilon_\alpha)P_\alpha, \quad (10)\\
&\cdots\\
&\cdots
\end{aligned}$$

When convergent, we have $V_{eff} = R_{n+1} = R_n$. The above non-degenerate LS method can be used to calculate the effective interactions for non-degenerate model spaces such as the two-shell space *sdpf*. But this method is rather complicated for computations, and this has hindered its application to microscopic calculations of shell-model effective interactions. To our knowledge, the above non-degenerate LS method has so far only been applied to the calculation of the $0p$-shell effective interactions [25].

We now describe some details of the non-degenerate KK and EKKO methods which are both suitable for the non-degenerate situation. The KK iteration method was originally developed for model spaces which are degenerate [10]. A non-degenerate KK iteration method was later formulated [11], with the effective interaction given by the following iteration methods. Let the effective interaction for the ith iteration be $V_{eff}^{(i)}$ and the corresponging eigenvalues E and eigenfunctions χ be given by

$$[PH_0P + V_{eff}^{(i)}]\chi_m^{(i)} = E_m^{(i)}\chi_m^{(i)}. \quad (11)$$

Here χ_m is the P-space projection of full-space eigenfunction Ψ_m, namely $\chi_m = P\Psi_m$. The effective interaction for the next iteration is then

$$V_{eff}^{(i+1)} = \Sigma_m[PH_0P + \hat{Q}(E_m^{(i)})]|\chi_m^{(i)}\rangle\langle\tilde{\chi}_m^{(i)}| - PH_0P, \quad (12)$$

where the bi-orthogonal states are defined by

$$\langle\chi_m|\chi_{m'}\rangle = \delta_{m,m'}. \quad (13)$$

Note that in the above PH_0P is non-degenerate. The converged eigenvalue E_m and eigenfunction χ_m satisfy the P-space self-consistent condition

$$(E_m(\omega) - H_0)\chi_m = \hat{Q}(\omega)\chi_m,\ \omega = E_m(\omega). \quad (14)$$

To start the iteration, we use

$$V_{eff}^{(1)} = \hat{Q}(\omega_0) \quad (15)$$

where ω_0 is a starting energy chosen to be close to PH_0P. The converged KK effective interaction is given by $V_{eff} = V_{eff}^{(n+1)} = V_{eff}^{(n)}$. When convergent, the resultant V_{eff} is independent of ω_0, as it is the states with maximum P-space overlaps which are selected by the KK method [10]. We shall discuss this feature later in section III using a solvable model. The above non-degenerate KK method is numerically more convenient than the non-degenerate LS method.

The diagrams of Fig. 1 have both one-body (d1,d2,d3) and two-body (d4,d5,d6,d7) diagrams. When we calculate nuclei with two valence nucleons such as ^{18}O and ^{18}F, all these seven diagrams are included for the $\hat{Q}$-box. But for nuclei with one valence nucleon such as ^{17}O, we deal with the 1-body $\hat{S}$-box such as the sum of diagrams d1, d2 and d3. The 1-body effective interaction is given by a similar KK iteration

$$S_{eff}^{(i+1)} = \Sigma_m[PH_0P + \hat{S}(E_m^{(i)})]|\chi_m^{(i)}\rangle\langle\tilde{\chi}_m^{(i)}| - PH_0P. \quad (16)$$

Denoting its converged value as S_{eff}, the model-space s.p. energy ϵ_m^{eff} is given by $P_m(H_0+S_{eff})P_m$. By adding and then subtracting S_{eff}, we can rewrite Eq.(14) as

$$(E_m(\omega) - H_0^{eff})\chi_m = [\hat{Q}(\omega) - S_{eff}]\chi_m,\ \omega = E_m(\omega), \tag{17}$$

with $H_0^{eff} = H_0 + S_{eff}$. In most shell model calculations [4, 5], one often uses the experimental s.p. energies. This treatment for the s.p. energies is in line with the above subtraction procedure, as $P(H_0 + S_{eff})P$ represents the physical s.p. energy which in principle can be extracted from experiments. In the present work we shall use the experimental s.p. energies for the model-space orbits together with the V_{eff} derived from $(\hat{Q} - S_{eff})$. A similar subtraction procedure has also been employed in the LS calculations [2, 3] where the all-order sum of the one-body diagrams were subtracted from the calculation of the effective interaction.

In several aspects, the above KK method provides a more desirable framework for effective interaction calculations than the commonly used LS method. The KK method can be more conveniently applied to non-degenerate model spaces than the LS method. In addition, high-order LS calculations requires high-order derivatives of the $\hat{Q}$-box which are often difficult to calculate, while in the KK method we do not need any $\hat{Q}$-box derivatives. But the KK method still has a short coming when applied to calculations with extended model space such as as the two-shell *sdpf* one. For example, certain 2nd-order diagrams for this case may become divergent, making the $\hat{Q}$-box divergent and disrupting the iteration method. It is remarkable that this singularity difficulty can be circumvented by the recently proposed EKKO method of Okamoto et al. [12]. In this method, the vertex function $\hat{Z}$-box is employed. It is related to the $\hat{Q}$-box by

$$\hat{Z}(\omega) = \frac{1}{1-\hat{Q}_1(\omega)}[\hat{Q}(\omega) - \hat{Q}_1(\omega)P(\omega - H_0)P], \tag{18}$$

where $\hat{Q}_1$ is the first-order derivative of the $\hat{Q}$-box. The $\hat{Z}$-box considered by Okamoto *et al.* [12] is for degenerate model spaces ($PH_0P = W_0$), while we consider here a more general case with non-degenerate PH_0P. An important property of the above $\hat{Z}$-box is that it is finite when $\hat{Q}$-box is singular (has poles). Note that $Z(\omega)$ satisfies

$$\hat{Z}(\omega)\chi_m = \hat{Q}(\omega)\chi_m \ at\ \omega = E_m(\omega). \tag{19}$$

The iteration method for determining the effective interaction for the $\hat{Z}$-box case is quite similar to that for the $\hat{Q}$-box. Suppose the effective interaction for the ith iteration is $V_{eff-Z}^{(i)}$. The corresponding eigenfunction χ and eigenvalues E^Z are determined by

$$[PH_0P + V_{eff-Z}^{(i)}]\chi_m^{(i)} = E_m^{Z(i)}\chi_m^{(i)}. \tag{20}$$

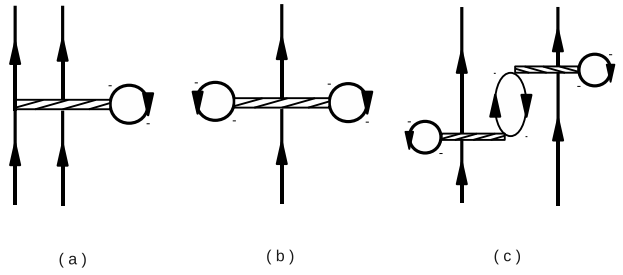

FIG. 2: $\hat{Q}$-box diagrams with three-nucleon forces. Each V_{3N}^{med} interaction is represented by a 'narrow band with hole-line-loop' vertex.

The effective interaction for the next iteration is

$$V_{eff-Z}^{(i+1)} = \Sigma_m[PH_0P + \hat{Z}(E_m^{Z(i)})]|\chi_m^{(i)}\rangle\langle\tilde{\chi}_m^{(i)}| - PH_0P, \tag{21}$$

where the χs are biorthogonal vectors ($\langle\chi_m|\chi_n\rangle = \delta_{mn}$). Although $\hat{Q}(\omega)$ and $\hat{Z}(\omega)$ are generally different, it is interesting that the converged eigenvalues E_m of $P(H_0 + V_{eff})P$ and the corresponding ones E_m^Z of $P(H_0 + V_{eff-Z})P$ are both exact eigenvalue of the full-space Hamiltonian $H = H_0 + V$ (this can be seen from Eqs.(14), (18) and (19)). Note, however, the KK and EKKO methods may reproduce different eigenvalues of the full-space Hamiltonian H. This aspect together with with some other comparisons of these methods will be discussed in section IIIa, using a simple solvable model.

For the degenerate case, Okamoto *et al.* [12] have shown that $\frac{dE_m^Z(\omega)}{d\omega}$ =0 at the self-consistent point $\omega = E_m^Z(\omega)$. As outlined below, we have found that this result also holds the case of non-degenerate PH_0P. From Eq.(18), we have

$$\frac{dZ}{d\omega} = \frac{1}{1-\hat{Q}_1}\hat{Q}_2\frac{1}{1-\hat{Q}_1}[\hat{Q} - \hat{Q}_1(\omega - H_0)] - \frac{1}{1-\hat{Q}_1}\hat{Q}_2(\omega - H_0). \tag{22}$$

Then from Eqs.(14) and (19) we have

$$[\frac{dZ(\omega)}{d\omega}]_{\omega=E_m^Z}|\chi_m\rangle = 0, \tag{23}$$

and

$$[\frac{dE_m^Z(\omega)}{d\omega}]_{\omega=E_m^Z} = 0. \tag{24}$$

This is a useful result; it states that at any self-consistent point the eigenvalues $E_m^Z(\omega)$ varies 'flatly' with ω, a feature certainly helpful to iterative calculations. In section III, we shall check this feature numerically.

We now describe how to include the effects of the leading-order chiral three-nucleon interaction, V_{3N}, in our calculations. We consider the NN interaction as given by $V = (V_{2N} + V_{3N}^{\rm med})$, where V_{2N} is the NN interaction obtained from the N^{3}LO Idaho two-body potential [24] and $V_{3N}^{\rm med}$ is a density-dependent two-body interaction

obtained from the chiral three nucleon (NNN) force by closing one pair of external lines and summing over the filled Fermi sea of nucleons. The leading contribution to V_{3N} occurs at N^{2}LO in the chiral power counting and is composed of a long-range two-pion exchange component $V_{3N}^{2\pi}$, a medium-range one-pion exchange term $V_{3N}^{1\pi}$, and a pure contact interaction V_{3N}^{ct}:

$$V_{3N}^{(2\pi)} = \sum_{i\neq j\neq k} \frac{g_A^2}{8f_\pi^4} \frac{\vec{\sigma}_i\cdot\vec{q}_i\,\vec{\sigma}_j\cdot\vec{q}_j}{(\vec{q}_i^{\,2}+m_\pi^2)(\vec{q}_j^{\,2}+m_\pi^2)} F_{ijk}^{\alpha\beta}\tau_i^\alpha\tau_j^\beta\,, \tag{25}$$

$$V_{3N}^{(1\pi)} = -\sum_{i\neq j\neq k} \frac{g_A c_D}{8f_\pi^4\Lambda_\chi} \frac{\vec{\sigma}_j\cdot\vec{q}_j}{\vec{q}_j^{\,2}+m_\pi^2} \vec{\sigma}_i\cdot\vec{q}_j\,\vec{\tau}_i\cdot\vec{\tau}_j, \tag{26}$$

$$V_{3N}^{(\mathrm{ct})} = \sum_{i\neq j\neq k} \frac{c_E}{2f_\pi^4\Lambda_\chi} \vec{\tau}_i\cdot\vec{\tau}_j, \tag{27}$$

where $g_A = 1.29$, $f_\pi = 92.4$ MeV, $\Lambda_\chi = 700$ MeV, $m_\pi = 138.04$ MeV$/c^2$ is the average pion mass, $\vec{q}_i = \vec{p}_i{}' - \vec{p}_i$ is the difference between the final and initial momentum of nucleon i and

$$\begin{aligned} F_{ijk}^{\alpha\beta} &= \delta^{\alpha\beta}\left(-4c_1m_\pi^2 + 2c_3\vec{q}_i\cdot\vec{q}_j\right) \\ &+ c_4\epsilon^{\alpha\beta\gamma}\tau_k^\gamma\vec{\sigma}_k\cdot(\vec{q}_i\times\vec{q}_j)\,. \end{aligned} \tag{28}$$

The low-energy constants $c_1 = -0.76\,\mathrm{GeV}^{-1}$, $c_3 = -4.78\,\mathrm{GeV}^{-1}$, and $c_4 = 3.96\,\mathrm{GeV}^{-1}$ appear already in the N^{2}LO two-nucleon potential and are therefore constrained by low-energy NN phase shifts [22]. The low-energy constants c_D and c_E are typically fit to reproduce the properties of light nuclei [16–18].

A general three-body force may be written in second quantization as

$$\hat{V}_{3N} = \frac{1}{36}\sum_{123456} V([123],[456]) b_1^\dagger b_2^\dagger b_3^\dagger b_6 b_5 b_4, \tag{29}$$

where the antisymmetrized matrix element is

$$V([123],[456]) \equiv \langle 123|V_{3N}|456+645+564-654-546-465\rangle. \tag{30}$$

Here $\langle 123|V_{3N}|456\rangle$ is a simple product matrix element, and $b^\dagger$ and b are creation and destruction operators defined with respect to the particle-hole vacuum $|C\rangle$ with $b_k|C\rangle = 0$ for all k. From eqs. (25-28) we can write $V_{3N} = V_{3N}^{(1)} + V_{3N}^{(2)} + V_{3N}^{(3)}$, where $V_{3N}^{(i)}$ is the component of V_{3N} that is symmetric with respect to the interchange $j \leftrightarrow k$. Now we contract one pair of the $b^\dagger$ and b operators of the above $\hat{V}_{3N}$ (both operators must be holes), and this leads to an effective two-body force

$$\hat{V}_{3N}^{\mathrm{med}} = \frac{1}{4}\sum_{1245} D([12],[45]) b_1^\dagger b_2^\dagger b_5 b_4, \tag{31}$$

with

$$\begin{aligned} D([12],[45]) &= \sum_{i\leq k_F}\Big[\langle i12|V_{3N}^{(2)}|i45\rangle + \langle 1i2|V_{3N}^{(2)}|4i5\rangle \\ &+ \langle 12i|V_{3N}^{(2)}|45i\rangle - \langle 1i2|V_{3N}^{(2)}|i45\rangle \\ &- \langle i12|V_{3N}^{(2)}|4i5\rangle - \langle 12i|V_{3N}^{(2)}|4i5\rangle \\ &- \langle 1i2|V_{3N}^{(2)}|45i\rangle + \langle i12|V_{3N}^{(2)}|45i\rangle \\ &+ \langle 12i|V_{3N}^{(2)}|i45\rangle - (4\leftrightarrow 5)\Big], \end{aligned} \tag{32}$$

where $4 \leftrightarrow 5$ denotes the nine exchange terms. The above result is unchanged when $V_{3N}^{(2)}$ is replaced by either $V_{3N}^{(1)}$ or $V_{3N}^{(3)}$. In our calculations we consider a background medium of symmetric nuclear matter at constant density characterized by a Fermi momentum k_F. In this way analytic expressions can be obtained for V_{3N}^{med}, as shown in refs. [19, 20]. The above is a density dependent effective 'two-nucleon' interaction which, unlike its underlying three-nucleon force, can be readily used in many-body problems.

As detailed in [20], the partial-wave potentials of the above V_{3N}^{med} have been derived from the lowest-order three-nucleon force. We shall use them in our calculations, namely we shall consider the nucleon interaction as given by $(V_{2N} + V_{3N}^{med})$. In so doing, the $\hat{Q}$-box diagrams for effective interactions will have a specific type of V_{3N} vertices as illustrated in Fig. 2. Recall that diagram d4 of Fig. 1 represents the interaction between two valence nucleons via V_{2N}. This diagram becomes diagram (a) of Fig. 2 if its V_{2N} is replaced by V_{3N}^{med}. Here the two valence nucleons have to have the participation of a sea-nucleon (below Fermi sea) in order to activate V_{3N}, as indicated by the hole-line loop in the diagram. Similarly diagram d1 of Fig. 1 represents the interaction of a valence nucleon with a sea-nucleon via the two-nucleon interaction V_{2N}. If this interaction is replaced by V_{3N}^{med}, this diagram becomes diagram (b) of Fig. 2. V_{3N} must involve three nucleons, and hence here the valence nucleon interacts with 'two' sea-nucleons as indicated by the two hole-line loops attached to V_{3N}. Diagram (c) is the V_{3N} core polarization diagram corresponding to diagram d7 of Fig. 1. Again here one hole-line loop is needed for each vertex to activate V_{3N}. As seen from Eqs. (31) and (32), V_{3N}^{med} requires the involvement of at least one sea-nucleon, and it is this requirement which is reflected by the hole-line loops attached to the V_{3N} vertices in Fig. 2.

III. RESULTS AND DISCUSSION

IIIa. Model calculations comparing the LS, KK and EKKO methods

In this section we shall study the above iteration methods by way of a simple matrix model, similar to the one employed in [12]. We consider a 4-dimensional matrix Hamiltonian $H = H_0 + H_1$ where

$$H_0 = \begin{bmatrix} PH_0P & 0 \\ 0 & QH_0Q \end{bmatrix} \tag{33}$$

and

$$PH_0P = \begin{bmatrix} \varepsilon_{p1} & 0 \\ 0 & \varepsilon_{p2} \end{bmatrix};\ QH_0Q = \begin{bmatrix} \varepsilon_{q1} & 0 \\ 0 & \varepsilon_{q2} \end{bmatrix}. \quad (34)$$

The interaction Hamiltonian has a strength parameter x, namely

$$H_1 = \begin{bmatrix} PH_1P & PH_1Q \\ QH_1P & QH_1Q \end{bmatrix}, \quad (35)$$

with

$$\begin{aligned} PH_1P &= \begin{bmatrix} 0 & 5x \\ 5x & 10x \end{bmatrix}; \\ PH_1Q &= QH_1P = \begin{bmatrix} 0 & 8x \\ 8x & 0 \end{bmatrix}; \\ QH_1Q &= \begin{bmatrix} -5x & x \\ x & -5x \end{bmatrix}. \end{aligned} \quad (36)$$

As discussed in section II, both the KK and EKKO iteration methods are rather convenient for non-degenerate model spaces. We would like to check this feature by carrying out some calculations using the above model. We consider two unperturbed Hamiltonians, given by $(\varepsilon_{p1},\ \varepsilon_{p2},\ \varepsilon_{q1},\ \varepsilon_{q2})$=(0,6,4,9) and (0,0,4,9). The PH_0P parts of them are, respectively, nodegenerate and degenerate.

In the first three entries of Table I, some results for the PH_0P=(0,6) case are presented. Here E_n are the exact eigenvalues of the full Hamiltonian, with their model-space overlaps denoted by $(n|P|n)$. E_{KK} and E_{EKKO} are the eigenvalues generated respectively by the KK and EKKO iterations methods. The above PH_0P not only is non-degenerate but also has its spectrum intersecting with that of QH_0Q. One would expect that this PH_0P may cause difficulty to the above iteration methods. But as indicated there, both the non-degenerate KK and the non-dgenerate EKKO iteration methods work remarkably well. Note that the interaction used here is rather strong (x=0.6), and both methods still work well, converging to values of E_ns which are quite far from PH_0P.

Some results for the degenerate case of PH_0P=(0,0) are listed in the last two entries of Table I. Here we have performed calculations using the degenerate LS method through 5th order iteration (i.e. in Eq.(7) we use $V_{eff} = R_5$). As shown, the results so obtained are not in good agreement with the exact results. This suggests that low-order LS iteration method may often be inadequate, and one needs higher-order iterations to obtain accurate results.

It has been known that the KK iteration method converges to the states with maximum P-space overlaps [10], while the LS method converges to the states of lowest energies [7, 8]. We have found that for many cases the EKKO method also converges to states of maximum P-space overlaps. As listed in the third entry of the Table, both the KK and EKKO methods converge to states of energies E_n= -3.51 and 14.53 whose P-space probabilties are relatively 0.70 an 0.86. We have also found that the EKKO and KK iteration methods can converge to different states. An example is the results shown in the last part of the Table, where the EKKO method converges to states of energy (P-space probability) -1.448 (0.868) and 0.906 (0.460) while the states of maximum probability are the first one and the third state with 5.254 (0.566). Note that for this case the EKKO method is clearly more accurate than the KK one.

We have noticed that for a number of cases the EKKO method converges well but not so for the KK method. This is largely because these two methods treat the singularities of the $\hat{Q}$-box differently. To see this, let us perform a graphical solution for the x=0.60 case of the Table. Using the parameters of this case, we calculate and plot in Fig. 3 $E^Q_m(\omega)$ and $E^Z_m(\omega)$ which are respectrively the eigenvalues of $P[H_0 + \hat{Q}(\omega)]P$ and $P[H_0 + \hat{Z}(\omega)]P$. As discussed in section II, they have identical self-consistent solutions, namely $\omega = E^Q_m(\omega) = E^Z_m(\omega) \equiv E_m$ where E_m is the eigenvalue of the full-space Hamiltonian. Recall that $\hat{Q}$ and $\hat{Z}$ are given respectively by Eqs. (2) and (18). As shown in the figure, the curves of E^Q and E^Z do have identical self-consistent solutions as marked by the common intersection points E_1, E_2, E_3 and E_4. Note that the above two curves are distinctively different from each other, particularly in the vicinity of the poles (marked by the vertical lines through F_1 and F_2) of the $\hat{Q}$-box. There $E^Q(\omega)$ is discontinuous, diverging oppositely before and after the pole, while $E^Z(\omega)$ remains continuous throughout. This clearly helps the convergence of the $\hat{Z}$-box iteration method: The $\hat{Z}$-box iteration proceeds along a continuous $E^Z(\omega)$ curve, while the $\hat{Q}$-box iteration often does not converge as it may bounce back and forth across the discontinuity.

As seen from Eq. (18), the $\hat{Z}$-box method has 'false' solutions at $E^Z_q(\omega) = \omega = \mu_q \equiv F_q$. These solutions are marked in Fig. 3 as F_1 and F_2. Thes false solutions can be readily recognized and discarded. As given in Eq.(24), we have at self-consistent points $\frac{dE^Z_m}{d\omega} = 0$. As shown in Fig. 3, the slopes of E^Z do satisfy the above condition at the self-consistent points E_1 to E_4, but not so at the false points F_1 and F_2.

IIIb. Nuclear matter and chiral NNN force

As described in section II, we shall calculate the shell-model effective interactions with the inclusion of the medium-dependent three-nucleon force V^{med}_{3N} which is obtained from a chiral NNN force by integrating one participating sea-nucleon over the Fermi sea. Before doing so, we need to choose or decide the low-energy constants of V_{3N} (see Eqs. (25-27)) to be used in our calculations. The low-energy constants c_1, c_3 and c_4 of $V^{(2\pi)}_{3N}$ are well determined; they are constrained by low-energy NN scat-

TABLE I: Results of model calculations using the LS, KK and EKKO iteration methods. See text for other explanations.

H_0= (0,6,4,9)	x=0.10			
E_n	-0.110705	3.328164	7.203243	8.579299
$(n\|P\|n)$	0.991108	0.044558	0.953368	0.010966
E_{KK}	-0.110705	7.203243		
E_{EKKO}	-0.110705	7.203242		
	x =0.30			
E_n	-0.974184	1.808716	8.080888	10.084581
$(n\|P\|n)$	0.906155	0.111257	0.113523	0.869066
E_{KK}	-0.974185	10.084580		
E_{EKKO}	-0.974185	10.084581		
	x =0.60			
E_n	-3.510377	-0.286183	8.265089	14.531471
$(n\|P\|n)$	0.709531	0.189318	0.232422	0.868729
E_{KK}	-3.510377	14.531472		
E_{EKKO}	-3.510363	14.531472		
H_0=(0,0,4,9)	x= 0.10			
E_n	-0.296201	0.982861	3.736229	8.577111
$(n\|P\|n)$	0.985416	0.922993	0.082811	0.008780
E_{LS}	-0.314591	0.872176		
E_{KK}	-0.296201	0.982860		
E_{EKKO}	-0.296201	0.982860		
	x= 0.30			
E_n	-1.448782	0.906504	5.254129	8.288149
$(n\|P\|n)$	0.868986	0.460296	0.566014	0.104704
E_{LS}	-1.620734	0.339561		
E_{KK}	-1.125579	5.515468		
E_{EKKO}	-1.448782	0.906504		

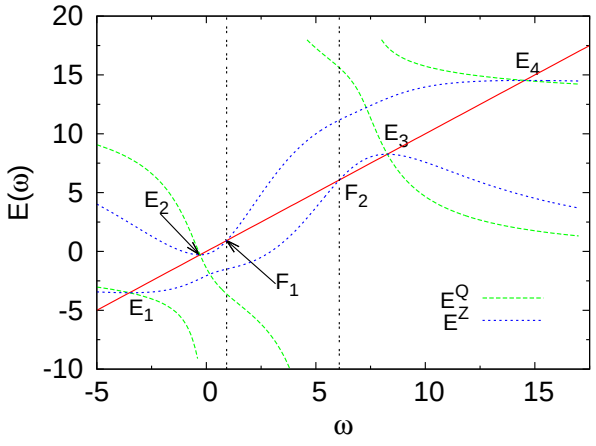

FIG. 3: Graphical solutions for the $\hat{Q}$- and $\hat{Z}$-box self-consistent equations. See text for other explanations.

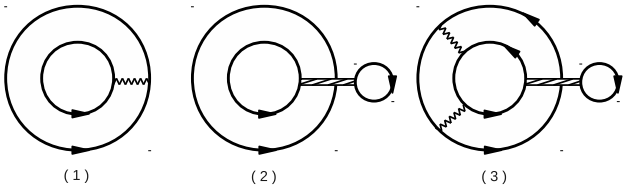

FIG. 4: Nuclear matter ring diagrams with vertices from V_{2N} (wavy line) and V_{3N}^{med} (narrow band with hole-line-loop).

tering data [22]. Their values so determined (section II) will be used in the present work. But the low-energy constants c_D and c_E, of $V_{3N}^{(1\pi)}$ and $V_{3N}^{(ct)}$ respectively, are less well known; their values determined from properties of light nuclei exhibit considerable variations [16–19]. The V_{3N}^{med} interaction depends explicitly on the Fermi momentum k_F which is well defined for nuclear matter. But k_F is not well defined for finite nuclei, causing uncertainty in determining the low-energy constants of V_{3N}^{med} from properties of finite nuclei. To circumvent this uncertainty, we have thus chosen to fix these constants by way of nuclear matter calculations with V_{3N}^{med} included. We fit the constants c_D and c_E by requiring them to reproduce satisfactorily the saturation density ρ_0 and energy per particle E_0/A of symmetric nuclear matter. It is convenient that k_F is well determined for nuclear matter. (It is not so for finite nuclei, for which we shall use a local density approximation for determining k_F as we shall discuss later.)

We calculate the equation of state (EOS) for symmetric nuclear matter using a ring-digram formalism [13–15]. A brief description of this formalism is presented below, to outline how we include V_{3N}^{med} in our calculations. In the above references, the low-momentum interaction $V_{low-k}(\Lambda)$ derived from two-nucleon realistic NN interactions was employed, Λ being the decimation scale. Our present ring-diagram calculations include in addition the interaction V_{3N}^{med}. Using familiar renormlization procedures [26–28] , we first obtain the low-momentum inbteraction $V_{low-k}^{3N}(\Lambda)$ from V_{3N}^{med}. Using the above ring-diagram framework, the ground-state energy shift ΔE is given by the all-order sum of the *pphh* ring diagrams as illustrated in Fig. 4. (ΔE_0 is defined as $(E_0 - E_0^{free})$ where E_0 is the true ground state energy and E_0^{free} that for the non-interacting system.) As shown in Fig.4, these ring diagrams contains vertices from both V_{low-k}^{2N} which is calculated from the N^{3}LO chiral NN potential [24] and V_{low-k}^{3N} obtained from the lowest order chiral V_{3N} as described in section II. Similar to Fig. 2, to have the pair of nucleons in the ring diagrams interact with V_{3N} there must be the participation of a third nucleon. Thus the V_{3N} vertices in Fig. 4 all have a one-hole-line loop attached to them.

With these ring diagram suumed to all orders, the

ground-state energy shift for nuclear matter is given as

$$\Delta E_0 = \int_0^1 d\lambda \sum_m \sum_{ijkl<\Lambda} Y_m(ij,\lambda) Y_m^*(kl,\lambda) \times \langle ij|[V_{low-k}^{2N}(\Lambda) + V_{low-k}^{3N}(\Lambda)]|kl\rangle. \quad (37)$$

The transition amplitudes above are $Y_m^*(kl,\lambda) = \langle \Psi_m(\lambda, A-2)|\beta(kl)|\Psi_0(\lambda, A)\rangle$, where $\Psi_0(\lambda, A)$ denotes the true ground state of nuclear matter which has A particles, $\Psi_m(\lambda, A-2)$ the mth true eigenstate of the $(A$-2) system, and $\beta(kl) = b_l b_k$ if $(k,l) > k_F$ and $= b_k^\dagger b_l^\dagger$ if $(k,l) \leq k_F$. Note that λ is a strength parameter, integrated from 0 to 1. The amplitudes Y are calculated from a RPA equation [13–15] based on the $(V_{2N}+V_{3N}^{med})$ interaction. Note that our calculation is the same as the usual Hartree-Fock (HF) one if we include only the 1st-order ring diagrams (1) and (2) of Fig. 4, and in this case the above Y amplitude becomes $Y(ij) = n_i n_j$ where n_i=1 for $i < k_F$ and =0 otherwise. Our ring-diagram calculations include particle-hole fluctuations of the Fermi sea, while not so for the HF calculations.

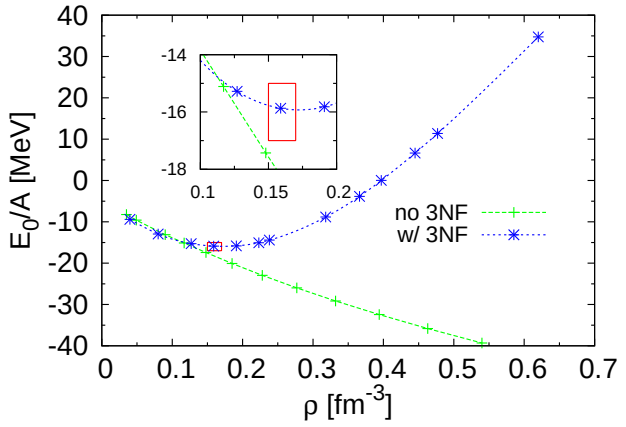

FIG. 5: Ring-diagram equation of state for symmetric nuclear matter calculated with and without V_{3N}.

We have carried out ring-diagram calculations for symmetric nuclear matter using a wide range values for c_D and c_E. Our results with $c_D = -2.8$ and $c_E = 0.7$ are displayed in Fig.5; they give $E_0/A \simeq -16$ MeV and $\rho_0 \simeq 0.16\ fm^{-3}$, both in satisfactory agreement with the empirical values. Two curves are shown in the figure, one with V_{2N} alone and the other with the addition of V_{3N}^{med}. Comparing with the V_{2N} curve, it is of interest that the effect of V_{3N}^{med} is slightly attractive for low densities ($<\sim 2\rho_0/3$) while becomes strongly repulsive at high densities. A common decimation scale of $\Lambda = 2.1\ fm^{-1}$ is used for both V_{low-k}^{2N} and V_{low-k}^{3N}. It may be mentioned that in the ring-diagram calculations with Brown-Rho scaling [13, 14] a larger Λ of $\sim 3.0 fm^{-1}$ is needed for obtaining satisfactory nuclear matter saturation properties. Further comparison of the Brown-Rho scaling with V_{3N} should be of interest, and we plan to study them in a future publication. The above c_D and c_E values will be employed in our shell model calculations.

We have calculated the HF s.p. spectrum ϵ_k in nuclear matter with the inclusion of both V_{2N} and three-nucleon force V_{3N}^{med}. The inclusion of the latter has been found to have significant effect to the spectrum. ϵ_k can be well fitted by the quadratic expression $(k^2\hbar^2/(2m^*) + \Delta)$ where m^* is the effective mass and Δ is a well-depth parameter representing the s.p. energy at zero momentum. In Fig. 6 we present our results for Δ and m/m^* for various densities. Two curves are shown: the lower one without and the top one with the inclusion of V_{3N}^{med}. The densities for the 7 data points of each curve are, from left to right, (0.25, 0.5, 1.0, 1.5, 2.0, 2.5, 3.0 ρ_0) respectively. As shown by the lower curve of the figure, Δ and m/m^* both vary monotonically with the density when only V_{2N} is employed. With increasing density, Δ becomes incresingly more negative and m/m^* increasingly larger, exhibiting no saturation. The trend is quite different for the upper curve where the three-nucleon force is included. Here m/m^* still monotonically increases with density, but Δ arises after saturation, approaching zero at some high density. It is of interest that V_{3N}^{med} has a large effect in raising the chemical potential of nucleons in high density nuclear matter; this raise of the chemical potential may play an important role in enabling such nucleons decaying into other baryons such as hyperons.

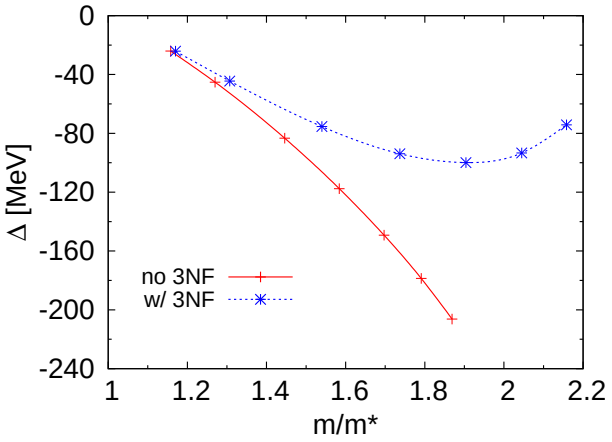

FIG. 6: Comparison of m^* and Δ for the in-medium s.p. spectrum calculated with and without V_{3N}^{med}. See text for other explanations.

IIIc. The *sdpf* shell model effective interactions

In this subsection, we shall calculate the effective interactions for both the degenerate *sd* one-shell and the non-degenerate *sdpf* two-shell cases. Before presenting our results, let us first describe some details of our calculations. The LS, KK and EKKO methods as described in section II will be employed. As also discussed in sec-

tion II, we first calculate the low-momentum interactions V_{2N}^{low-k} and V_{3N}^{low-k} from, respectively, the chiral V_{2N} and V_{3N}^{med} potentials, using a common decimation scale of $\Lambda = 2.1\ fm^{-1}$ for both. This value was chosen because at this scale the low-momentum interactions derived from different NN potentials [24, 29–31] are remarkably close to each other, leading to a nearly unique low-momentum interacton. The above V_{2N}^{low-k} and V_{3N}^{low-k} interactions are then used in calculating the $\hat{Q}$-box diagrams as shown in Figs. 1 and 2. In calculating these diagrams, the hole orbits are summed over the $0s0p$ shells and particle orbits over the $0d1s1p0f$ shells. The active spaces (P-space) used for the one-shell and two-shell calculations are respectively the three orbits in the *sd* shell and the seven orbits in the *sdpf* shells. The experimental s.p. energies of (0.0, 5.08, 0.87) MeV have been used, respectively, for the $(0d_{5/2}, 0d_{3/2}, 1s_{1/2})$ orbits [32]. The harmonic oscillator constant of $\hbar\omega$=14 MeV has been employed in our calculations.

In Figs. 7 and 8 we compare our *sd* one-shell calculations using V_{2N} only. Here our purpose is mainly to compare the results given by the KK and EKKO method with those given by the commonly used degenerate LS method [2, 3]. To our knowledge, the KK and EKKO methods have not yet been applied to calculations of shell-model effective interactions. It should be useful and of interest to compare the results given by the LS, KK and EKKO methods. Our LS calculations are carried out using a low-order approximation, namely we take $V_{eff} = R_5$ (see Eq.(7)). For simplicity, we shall just use in our present and subsequent calculations a low-order $\hat{Q}$-box as indicated by the 1st- and 2nd-order diagrams of Figs. 1 and 2. As shown in Figs. 7 and 8, the KK and EKKO results for both ^{18}O and ^{18}F are in fact identical to each other, which is consistent with our model calculations displayed in Table I and Fig. 3. For these two methods, we have used both iteration and graphical methods, to ensure the convergence of the iterative results.

As displayed in Figs. 7 and 8, it is encouraging that the low-order ($V_{eff} = R_5$) LS method has given results in very good agreement with the KK and EKKO ones. This is possibly because the P- and Q-space employed in the present calculation are not strongly coupled; they have a separation of $2\hbar\omega$. (The model calculations considered in Table I have much stronger P- and Q-space couplings.) A comparison of our results with experiments [32] is also presented in Figs. 7 and 8. The agreement between our calculated energy levels with experiments is moderately satisfactory for ^{18}O, but for ^{18}F the calculated lowest $(1^+, 3^+, 5^+)$ states, though of correct ordering, are all significantly higher than the experimental values. As discussed in section IIIa, the LS method is known to converge to the states of the lowest energies, while the KK method to the states of maximum P-space overlaps. Thus the good agreement between LS and KK in Figs. 7 and 8 is an important indication that the states

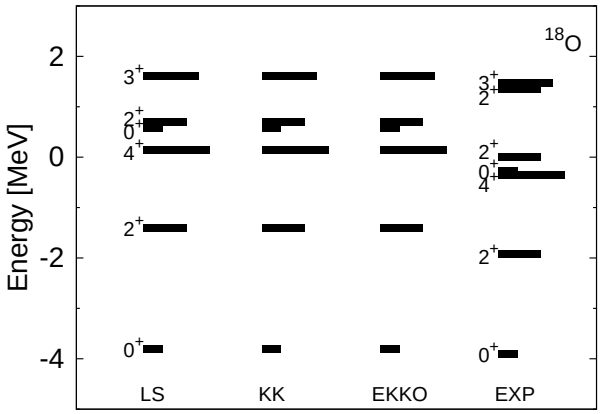

FIG. 7: Energy spectrum of ^{18}O obtained from *sd*-shell calculations using the LS, KK and EKKO methods, all employing only V_{2N}.

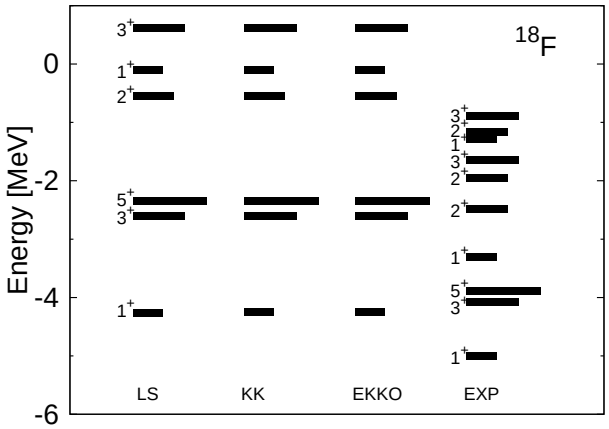

FIG. 8: Same as Fig. 7 except for ^{18}F.

reproduced by the model-space effective interaction are likely those of the lowest energies as well as maximum model-space overlaps. It is certainly physically desirable to have the effective interaction reproducing the states of the full Hamiltonian which have the largest model-space overlaps.

We now turn to the effect of three-nucleon potential V_{3N}^{med} on the shell-model effective interactions. As an initial study, we repeat the one-shell calculations of Figs. 7 and 8 with the interaction V_{2N} used there replaced by $(V_{2N} + V_{3N}^{med})$. The results so obtained clearly depends on what V_{3N} we employ. As discussed in section IIIb the low-energy constants c_1, c_3 and c_4 are well constrained by NN scattering data, and for the constants c_d and c_E we have chosen to use their values determined by nuclear matter properties. To carry on the calculations with V_{3N}^{med} we still need to know the 'local density' ρ_v for the two valence nucleons in the *sd* shell. It should be small, but its precise value is rather uncertain. In the present work, we shall estimate ρ_v by comparing the den-

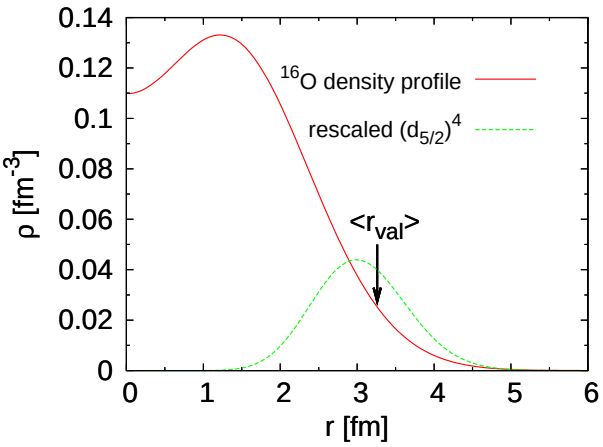

FIG. 9: Density profile of ^{16}O (solid line) and the radial distribution of the fourth power of the 0d shell-model wave function (dashed line). See text for other explanations.

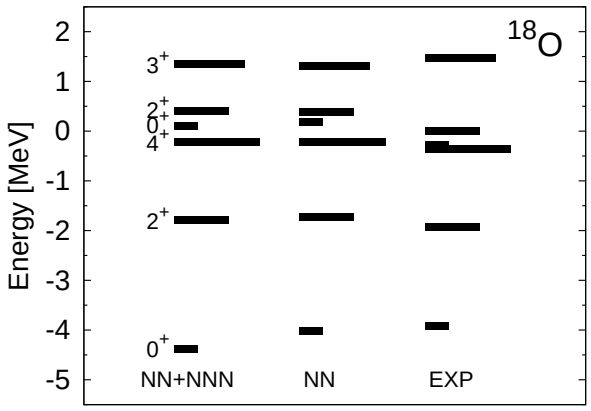

FIG. 10: Energy spectra of ^{18}O calculated with the *sd* one-shell effective interactions. 'NN' and 'NNN' denote respectively V_{2N} and V_{3N}^{med}.

sity profile of ^{16}O and that for the valence nucleons. In Fig. 9 we plot the density profile $\rho_{core}(r)$ of ^{16}O obtained with its wave function assumed to be a closed shell-model s^4p^{12} core. We also plot the distribution $\Phi(r) = \xi\phi(r)^4$ where $\phi(r)$ is the radial harmonic oscillator wave function for $d_{5/2}$, with the scaling parameter ξ=0.1. As seen from the plots, the pair of $d_{5/2}$ nucleons reside primarily in the low-density region of ρ_{core}. Depending on the averaging procedure employed, we have estimated ρ_v from $\rho_{core}(r)$ and $\phi(r)$, obtaining values ranging from ~ 0.015 to $\sim 0.030 fm^{-3}$. We have considered another scheme to estimate ρ_v. The rms radius $< r_{val} >$ for the shell-model $d_{5/2}$ orbit is indicated by an arrow in the figure. A simple scheme to estimate ρ_v is to let it equal to $\rho_{core}(< r_{val} >)$, the value obtained in this way being $\sim 0.025 fm^{-3}$. This value may be reduced if realistic s.p. wave functions are employed. The $d_{3/2}$ orbit is nearly unbound, and its rms radius should be considerably larger than that for $d_{5/2}$.

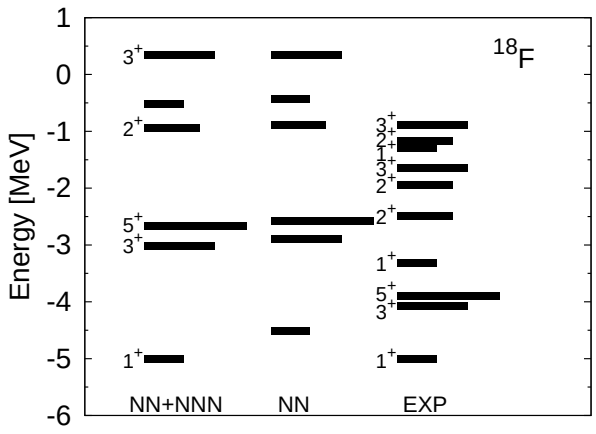

FIG. 11: Same as Fig. 10 except for ^{18}F.

Assuming $\hbar\omega$ =10 MeV for the $d_{3/2}$ orbit, its $< r_{val} >$ would be $\sim 3.8 fm$ giving $\rho_v \simeq 0.01 fm^{-3}$ for this orbit. We believe that a suitable range for ρ_v is from ~ 0.1 to $\sim 0.2\rho_0$ ($\rho_0 \equiv 0.16 fm^{-3}$).

In Figs. 10 and 11, we present our results for ^{18}O and ^{18}F calculated with and without V_{3N}^{med} ($\rho_v = 0.15\rho_0$). Comparing with the 'NN' results, the main effect of the 'NNN' force is a small downward shift for the ground states of ^{18}O and ^{18}F, while leaving the other states largely unchanged. This trend is consistent with what we have observed for nuclear matter calculations (see Fig. 5), namely the effect of V_{3N}^{med} is slightly attractive at low densities. With the inclusion of thre 'NNN' force, the ground-state energy of ^{18}F is in good agreement with experiment while that for ^{18}O is slightly overbound. It may be mentioned that we have employed a low-order approximation for the $\hat{Q}$-box, including only 1st- and 2nd-order diagrams. The inclusion of higher-order diagrams may alter our results. As carried out by by Holt et al. [33], certain classes of planar diagrams of the $\hat{Q}$-box can be summed up to all orders using the Kirson-Babu-Brown induced interaction method. We plan to extend our present calculations by including these planar diagrams in the $\hat{Q}$-box.

Let us now describe our calculations for the non-degenerate *sdpf* effective interactions. The shell-model calculations of Figs. 7-8 and 10-11 have all been carried out using the *sd* one-shell model space. For certain nuclei such as those with a large neutron excess, a larger model space such as the *sdpf* one may be needed and therefore the above effective interactions will be required. It may be convenient to descibe our *sdpf* calculations by way of an example, namely ^{18}O. Consider the $(T = 1, J = 0)$ states of this nucleus. In the *sd* one-shell case, the model space is spanned by three basis states $|j^2, T = 1, J = 0\rangle$, j=$(d_{5/2}, d_{3/2}, s_{1/2})$. For the *sdpf* case, the model space is enlarged, having four additional basis states of the same type with j=$(p_{3/2}, p_{1/2}, f_{7/2}, f_{5/2})$. The whole model space is now non-degenerate as the *pf*

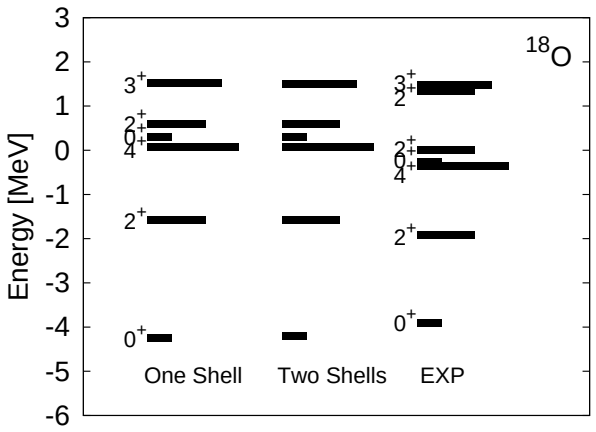

FIG. 12: Comparison of the ^{18}O spectra calculated from the *sd* one-shell and *sdpf* two-shell effective interactions. Both with V_{3N}.

orbits are one shell above the *sd* ones. We shall employ the non-degenerate KK and EKKO methods to calculate the effective interactions for this two-shell space. As illustrated in section IIIa, both of these methods have been applied to non-degenerate model calculations. Here we would like to study if they are also suitable for calculating non-degenerate shell model effective interactions.

Our results for the *sdpf* calculations for ^{18}O are presented in Fig. 12. The effective interaction used here is calculated in the same way as those used in the 'NN+NNN' columns of Figs. 10-11 except for the few differences related to the use of the larger model space. With the *sdpf* space, the second-order $\hat{Q}$-box diagrams d5 of Fig. 1 and similar ones with the V_{3N}^{med} vertices are no longer needed as their intermdediate states are already within the model space. For the *sd* one-shell case, we have employed the experimental s.p. energies for the three *sd*-shell orbits. (See section IIIb.) For the *sdpf* situation, we need in addition the experimental s.p. energies for the four *pf* orbits. Their values are, however, not well known. In the present calculation we have placed them all at one $\hbar\omega$ (14 MeV) above the $d_{5/2}$ level. (In the preceeding *sd* calculation the same separation is used between the unperturbed *pf* and *sd* orbits.) As shown in Fig. 12, we compare our 'One Shell' (*sd*) and 'Two Shells' (*sdpf*) results; it is of interest that they agree with each other rather well. Similar good agreement has also been observed for the corresponding ^{18}F calculations. We have found that this good agreement is largely due to the core polarization effects included in the $\hat{Q}$-box. The above comparisons provide in fact a test of our calculations. The renormalized *sd* and *sdpf* effective intertactions are different, but in principle some of the eigenvalues given by the *sdpf* interactions should also be the eigenvalues given by the *sd* interactions. We have found in our calculations that the energies for the states with maximum *sd* overlaps given by the *sdpf* effective interactions are all in close agreement with the corresponding ones given by the *sd* effective interactions. Our *sdpf* effective interactions have been calculated using both the KK and EKKO methods, obtaining practically identical results. In short, we believe that these two methods are both well suited for calculating the shell-model effective interactions for non-degenerate model spaces. In the present work we have only made an initial application, in calculating the low-lying states of ^{18}O and ^{18}F. Further applications of these methods should be of interest.

IV. SUMMARY AND OUTLOOKS

The iteration method of Krenciglowa and Kuo (KK) and that recently developed by Okamoto et al. (EKKO) are applied to the microscopic derivations of the *sd* and *sdpf* shell-model effective interactions using the chiral two-nucleon (V_{2N}) and three-nucleon (V_{3N}) potentials. We first study these two methods using a solvable model, and find that they are both suitable and efficient for deriving the effective interactions for non-degenerate model spaces, including the situation where the P-space and Q-space unperturbed Hamiltonians have spectrum overlaps. The Lee-Susuki (LS) iteration method, which has been widely used for deriving degenerate shell-model effective interaction, is not as convenient as the KK and EKKO methods for the non-degenerate situation. The EKKO method has a special advantage that its vertex function $\hat{Z}$-box is, by construction, a continuous function while the $\hat{Q}$-box function used in LS and KK may have singularities. This is helpful to the convergence of the EKKO iteration method.

Using V_{2N} alone, we first calculate the degenerate *sd*-shell effective interactions using all LS, KK and EKKO methods. The results given by KK and EKKO are identical. It is noteworthy that the LS results, calculated with a low-order (5th order) iteration, are in very good agreement with the KK and EKKO ones, supporting the accuracy of the low-order LS method for calculating the degenerate shell-model effective interactions. We have calculated the non-degenerate *sdpf* effective interactions using V_{2N} with and without the inclusion of V_{3N} using both KK and EKKO methods. We believe that these methods are both suitable for microscopic calculations of non-degenerate effective interactions. Our results for the *sdpf* effective interactions given by the KK and EKKO methods are practically equivalent to each other. The low-lying states of ^{18}O and ^{18}F given by the *sdpf* effective interactions are nearly the same as those by the *sd* ones.

In our calculations we have employed the three-nucleon force V_{3N}^{med} which is obtained from V_{3N} by integrating one of its participating nucleons over the Fermi sea, as indicated by the 'hole-line' loops in Figs. 2 and 4. We have carried out calculations for symmetric nuclear matter with the inclusion of this interaction and determine

its low-energy constants c_D and c_E by requiring them to give satisfactory nuclear matter saturation properties. V_{3N}^{med} is explicitly dependent of the density ρ of the nuclear medium, and there is uncertainty in determining its value appropriate for the effective interactions among valence nucleons. In the present work we have obtained this value using averaging methods based on the density profile of ^{16}O and the radial distribution of valence nucleons. This is an approximate treatment which should be further investigated and improved upon. We have carried out calculations for ^{18}O and ^{18}F using V_{2N} with and without the above V_{3N}^{med}, the main effect of the latter being a small downward shift for the ground states of these nuclei while leaving the other states essentially unchanged.

We are very grateful to L. Coraggio, A. Covello, A. Gargano, N. Itaco, M. Machleidt and R. Okamoto for many helpful discussions. Partial supports from the US Department of Energy under contracts DE-FG02-88ER40388 and the DFG (Deutsche Forschungsgemeinschaft) cluster of excellence: Origin and Structure of the Universe are gratefully acknowledged.

[1] T. T. S. Kuo and E. Osnes, *Lecture Notes in Physics* (Springer-Verlag, New York, 1990), Vol. 364.
[2] M. Hjorth-Jensen, T. T. S. Kuo, and E. Osnes, Phys. Rep. **261**, 126 (1995), and references therein.
[3] L. Coraggio, A. Covello, A. Gargano, N. Itaco and T.T.S. Kuo, Prog. Part. Nucl. Phys., 62 (2009) 135, and references quoted therein.
[4] B.A. Brown and B.H. Wildenthal, Ann. Rev. Nucl. Part. Sci. **38**, 29(1988).
[5] B.A. Brown, W.A. Richter, Phys. Rev. C74, 0343150 (2006).
[6] T.T.S. Kuo, S.Y. Lee and K.F. Ratcliff, *Nucl. Phys.* **A176** (1971) 172.
[7] S.Y. Lee and K. Suzuki, *Phys. lett.* **91B**, 173 (1980).
[8] K. Suzuki and S.Y. Lee, *Prog. Theor. Phys.* **64**, 2091 (1980).
[9] K. Suzuki, R. Okamoto, P.J. Ellis and T.T.S. Kuo, *Nucl. Phys.* **A567** (1994) 576.
[10] E.M. Krenciglowa and T.T.S. Kuo, *Nucl. Phys.* **A235**, 171 (1974).
[11] T.T.S. Kuo, F. Krmpotic, K. Suzuki and R. Okamoto, *Nucl. Phys.* **A582**, 205(1995).
[12] R. Okamoto, K. Suzuki, H. Kumagai and S. Fujii, to be published in 'Proceedings of the 10th International Spring Seminar on Nuclear Physics (May 21-25, Sur Mare Vietri, Italy, ed. by A. Covello)'; [nucl-th] arXiv:1011.1994v1.
[13] L.W. Siu, J.W. Holt, T.T.S. Kuo and G.E. Brown, Phys. Rev. **C79**, 054004 (2009).
[14] H. Dong, T.T.S. Kuo and R. Machleidt, Phys. Rev. **C80**, 065803 (2009).
[15] H. Q. Song, S. D. Yang and T.T.S. Kuo, Nucl. Phys. **A462**, 491 (1987).
[16] A. Nogga, H. Kamada and W. Glockle, Phys. Rev. Lett. **94**, 944(2000).
[17] S.C. Peiper, K. Varga and R. B. Waringa, Phys. Rev. **C66**, 044310 (2002).
[18] P. Navratil, V.G. Gueorguiev, J.P. Vary, W.E. Ormand and A. Nogga, Phys. Rev. Lett. **99**, 042501(2007).
[19] J. W. Holt, N. Kaiser and W. Weise, Phys. Rev. **C79**, 054331 (2009).
[20] J. W. Holt, N. Kaiser and W. Weise, Phys. Rev. **C81**, 024002 (2010).
[21] T. Otsuka, T. Sizuki, J.D. Holt, A. Schwenk and Y. Akaishi, Phys. Rev. Lett. **105**, 032501 (2010).
[22] M. C. M. Rentmeester, R. G. E. Timmermans, and J. J. de Swart, Phys. Rev. C **67** (2003) 044001.
[23] E. Epelbaum, Prog. Part. Nucl. Phys. **57**, 654(2006).
[24] D. R. Entem, R. Machleidt, and H. Witala, Phys. Rev. C **65**, 064005 (2002).
[25] L. Coraggio and N. Itaco, Phys. Lett. **B616**, 43 (2005).
[26] S. K. Bogner, T. T. S. Kuo and L. Coraggio, Nucl. Phys. **A684**, (2001) 432.
[27] S.K. Bogner, T.T.S. Kuo, L. Coraggio A. Covello, and N. Itaco, Phys. Rev. C **65**, 051301(R) (2002).
[28] S. K. Bogner, T. T. S. Kuo, and A. Schwenk, Phys. Rep. **386**, 1 (2003).
[29] R. Machleidt, Phys. Rev. C **63**, 024001 (2001).
[30] R. B. Wiringa, V. G. J. Stoks, and R. Schiavilla, Phys. Rev. C **51**, 38 (1995).
[31] V. G. J. Stoks, R. A. M. Klomp, C. P. F. Terheggen, and J. J. de Swart, Phys. Rev. C **49**, 2950 (1994).
[32] http://www.nndc.bnl.gov/chart/.
[33] J. W. Holt, G. E. Brown, J. D. Holt and T. T. S. Kuo, Nuc. Phys. A785 (2007) 322.